Spatial mismatch between the Na^+ flux and spike initiation in axon initial segment

Gytis Baranauskas[1], Yaron David[1], and Ilya A. Fleidervish[2]

Department of Physiology and Cell Biology, Faculty of Health Sciences and Zlotowski Center for Neuroscience, Ben-Gurion University of the Negev, Beer Sheva 84105, Israel

Edited by Eve Marder, Brandeis University, Waltham, MA, and approved December 26, 2012 (received for review August 31, 2012)

It is widely believed that, in cortical pyramidal cells, action potentials (APs) initiate in the distal portion of axon initial segment (AIS) because that is where Na^+ channel density is highest. To investigate the relationship between the density of Na^+ channels and the spatiotemporal pattern of AP initiation, we simultaneously recorded Na^+ flux and action currents along the proximal axonal length. We found that functional Na^+ channel density is approximately four times lower in the AP trigger zone than in the middle of the AIS, where it is highest. Computational analysis of AP initiation revealed a paradoxical mismatch between the AP threshold and Na^+ channel density, which could be explained by the lopsided capacitive load imposed on the proximal end of the AIS by the somatodendritic compartment. Favorable conditions for AP initiation are therefore achieved in the distal AIS portion, close to the edge of myelin, where the current source–load ratio is highest. Our findings suggest that cable properties play a central role in determining where the AP starts, such that small plastic changes in the local AIS Na^+ channel density could have a large influence on neuronal excitability as a whole.

neocortex | pyramidal neuron | sodium imaging

In cortical pyramidal cells, as in many CNS neurons, action potentials (APs) generally initiate in the axon initial segment (AIS) (refs. 1-4; reviewed in ref. 5), the proximal part of the axon where the neuronal membrane is not covered with a myelin sheath, and which possesses a distinctive, specialized assembly of voltage-gated channels and associated proteins (6). Because of the pivotal role that the AIS plays in transformation of synaptic input into AP output, precise characterization of its excitable properties is essential for a complete understanding of the cellular mechanisms that underlie operation of cortical neurons and networks. Early theoretical studies proposed two mechanisms to explain preferential AIS AP initiation (7, 8): (*i*) less current is required to depolarize the AIS membrane to threshold because it is electrically isolated from the neighboring neuronal compartments, and (*ii*) the depolarizing current density is higher in the AIS than in neighboring compartments, allowing the AIS to overcome their electric load. These two mechanisms are not mutually exclusive, but the technical difficulties that hinder precise measurements in thin neuronal processes have made it difficult to elucidate their relative importance for AP initiation.

During the past decade, the isolation hypothesis has been addressed by only a few studies (9), and values of the relevant resistances and capacitances are only approximations. By contrast, the findings by many groups that Na^+ channel density is relatively high in the proximal axon have focused most attention on the higher current hypothesis, although there remains some controversy as to what extent the density of functional Na^+ channels is greater in the AIS than in the soma (refs. 10–14; reviewed in ref. 15). The role of high AIS current density is supported by evidence that axonal Na^+ channels possess specialized kinetic properties, including more hyperpolarized activation voltage (10, 11, 13, 16), faster activation (17), and a higher propensity to generate persistent Na^+ current (14, 18, 19).

All this evidence seems to suggest that the AP trigger zone in the AIS is also the site of highest Na^+ current density. To determine whether this is indeed the case, we used high-speed Na^+ imaging combined with axonal action current electrical recordings to quantitatively describe the Na^+ influx and the spatiotemporal pattern of AP initiation along the proximal axon. Our previous imaging experiments using trains of 5 to 10 APs to elicit the Na^+ signals (14), as well as evidence from others (11), showed that Na^+ influx is maximal in the central portion of the AIS. In these experiments, however, the extent of flux variations was not quantitatively established, as interpretation of the imaging data from the most proximal and most distal parts of the AIS was complicated by somatic light scattering and by rapid Na^+ diffusion during the AP trains. Here, we substantially improved the spatial and temporal resolution by lowering the temperature and comparing the distribution of Na^+ transients with that of submillisecond differences in AP latency measured by using loose patch-clamp technique. We limited the present study to Na^+ signals elicited by single APs, as the peak amplitude of these signals should almost be unaffected by lateral diffusion and therefore could be taken as a measure of local Na^+ entry. We now report that, in the actual trigger zone, which is located in the most distal 10 μm of the 40- to 60-μm AIS, functional Na^+ channel density is approximately four times lower than in the middle of the AIS, where it is highest. We conclude that, in cortical pyramidal neurons, the AP is first triggered at the site that is most electrically isolated from the adjacent soma, and not where the Na^+ current density is highest.

Results

We recorded changes in the fluorescence of the Na^+-sensitive dye sodium-binding benzofuran isophthalate (SBFI) (20) in soma and proximal axon of large layer 5 pyramidal neurons in slices of mouse somatosensory cortex. Fig. 1*A* (*Top*) shows a typical neuron as seen during the imaging experiment. In this and 11 other SBFI-filled neurons, fluorescence intensity measurements confirmed that the dye concentration within the somatic and proximal axonal compartments was nearly uniform. The gradual decline in the fluorescence intensity from its maximal value in the center-middle region of the soma to a minimum at ~20 μm of the axonal length (Fig. 1*A*, *Bottom*) can be attributed to (*i*) the gradual decrease in somatic depth from the center toward periphery (*ii*), tapering of the axon within the first 20 μm of its length, and (*iii*) scattering of light emitted from the soma, which was 10 to 20 times brighter than the axon. In

Author contributions: G.B. and I.A.F. designed research; G.B., Y.D., and I.A.F. performed research; G.B., Y.D., and I.A.F. analyzed data; and I.A.F. wrote the paper.

The authors declare no conflict of interest.

This article is a PNAS Direct Submission.

See Commentary on page 3715.

[1]G.B. and Y.D. contributed equally to this work.

[2]To whom correspondence should be addressed. E-mail: ilya@bgu.ac.il.

This article contains supporting information online at www.pnas.org/lookup/suppl/doi:10.1073/pnas.1215125110/-/DCSupplemental.

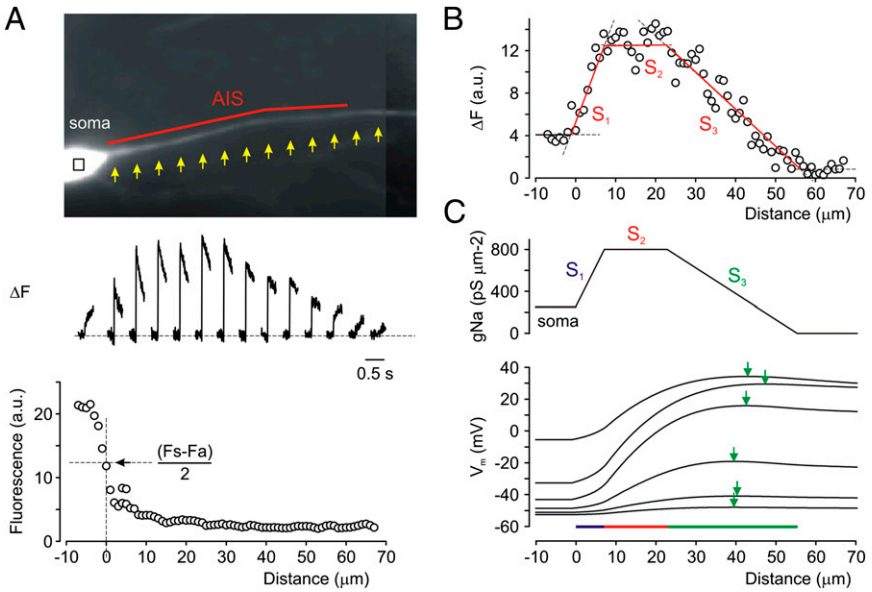

Fig. 1. Distribution of AP evoked Na^+ flux along the soma–axon axis. (*A*, *Top*) Representative neuron as seen during the imaging experiment with the NeuroCCD-SMQ camera. The rectangle and arrows indicate the regions from where fluorescence measurements were obtained. Red line indicates the axonal region where fast-increasing fluorescent signals were detected. (*Middle*) Averaged ΔF transients ($n = 60$) elicited by a single AP in the indicated region in the soma and in the 5-μm-long axonal segments. (*Bottom*) Total SBFI fluorescence measured along the soma–axon axis. The half-difference of the somatic and axonal fluorescence (dashed lines) was assigned as zero point for the axonal length measurements. (*B*) AP evoked Na^+ flux in the soma and axon of a layer 5 pyramidal neuron. Dots are averaged peak ΔF values from 1-μm-long pixels in the soma and along the axon. Dashed lines are linear fits to the data; continuous lines designate the slope of Na^+ influx as a function of distance in the soma (black) and in the incrementing, steady, and decreasing flux subsegments of the AIS (red; S_1, S_2, and S_3, respectively). (*C*) In a model with Na^+ channel distribution based on measured Na^+ fluxes, AP initiates in the distal AIS (S_3), outside of the maximal Na^+ influx subsegment, S_2. Voltage–distance plots along the soma–axon axis shown at time intervals of 50 μs. Green arrows indicate positions of maximum voltage. Relative S_1, S_2, and S_3 position are color-coded as blue, red, and green, respectively.

morphological studies, the point of onset of the dense granular material underlying the surface membrane (21) or the proximal boundary of expression of the axon-specific anchoring proteins (10) is usually taken as a point of the AIS origin from the cell body. As these morphological landmarks are not available in live cell recordings, we assigned half-difference of the somatic and axonal fluorescence as the zero point of the axonal length. In all cells studied, this point roughly corresponded to the edge of soma, as seen with IR differential interference contrast optics.

We previously showed that the dynamics of Na^+ transients for short times can be entirely described in terms of ion influx and diffusion (14). In the present study, we minimized the effect of diffusion by using only single APs to generate increases in intracellular Na^+ concentration ($[Na^+]_i$). We measured the absolute change in fluorescence (ΔF), which is proportional to the Na^+ influx per unit membrane area (14) and is relatively unaffected by the somatic light scattering and background tissue fluorescence. The fluorescence signals in the AIS increased very sharply, reaching a peak at approximately 3 ms after the peak of the somatic AP, which is quite close to the time of peak $[Na^+]_i$ predicted by the diffusion model (Fig. S1). Spatially, peak amplitude of the averaged ΔF transients grew over the first 10 μm of axonal length, reaching a maximal value approximately three times greater than the somatic ΔF in a ∼20-μm-long central segment of the AIS, and then decreasing gradually to nearly zero in the presumed myelinated region (Fig. 1*A*, *Middle*). Thus, in terms of Na^+ influx, the AIS could be subdivided into the three subsegments: S_1 with incrementing Na^+ channel flux, S_2 with a steady maximal flux, and S_3 with decreasing flux density (Fig. 1*B*). Of a total AIS length of 43 ± 11 μm (mean ± SD; $n = 12$), S_1 extended 8 ± 3 μm from the soma, S_2 continued for a further 14 ± 5 μm, and S_3 extended for a further 21 ± 7 μm to the edge of the myelin. Interestingly, the main source of variance in total AIS length was variance in the length of the S_3 subsegment (range, 14–34 μm), whereas the length of the proximal subsegments was generally constant within the sampled neuronal population. The peak amplitude of the ΔF change within S_2 was 2.3 ± 0.3 ($n = 12$) times greater than in the soma. Such spatial Na^+ flux pattern was found sufficient to account for the experimentally observed and simulated $[Na^+]_i$ changes elicited by single AP in the AIS (Fig. S2*A*).

The assumption that Na^+ channel density is uniform over the AIS, however, was found not to be valid, as the simulated $[Na^+]_i$ pattern differed considerably from the experimentally observed ΔF/F in S_1 and S_3 (Fig. S2*A*). The simulations also confirmed that, within the brief time window following the spike, when our measurements were made, diffusion-associated distortion of Na^+–AIS length relationship is indeed minimal. As ΔF is proportional to the density of the flux per unit membrane area, we sought to find out whether the larger surface area within the most proximal AIS could compensate for the smaller flux density. Multiplying the flux-proportional parameter, ΔF, by a parameter proportional to the axon surface area, $\sqrt{F}$, resulted in absolute flux distribution (Fig. S2*B*) that was not significantly different from that of Fig. 1*B*. Although it has been suggested that Na^+ channels may be unevenly distributed in the membrane by forming clusters a few micrometers in diameter, careful analysis showed that the spatial, amplitude, and temporal resolution of our optical recordings was insufficient to reveal such clusters (22), if they exist (Fig. S3).

The ability of the neuronal membrane at any given location to generate AP depends not only on the size and duration of its Na^+ conductance but also on the electrical load presented to it by the neighboring compartments (7). We therefore studied the dynamics of AP initiation in a simplified compartmental model in which we distributed Na^+ conductance along the axosomatic axis in accordance with our measurements. In good agreement with earlier reports (1, 4), brief current steps in the soma elicited APs that were first initiated at a distance of approximately 40 μm

from the soma, in the middle of the S_3, beyond the site of highest Na^+ conductance (Fig. 1*C*). The lowest threshold for AP initiation in the distal AIS was not because of a leftward shift in activation threshold of the more distal channels (10), as our model assumed uniform gating properties for all axonal Na^+ channels. Analysis of the model behavior revealed that the spatial mismatch between the Na^+ flux and AP initiation was a reflection of the complex electrotonic interactions that exist within the AIS and between the AIS and neighboring compartments (7, 8). The AIS itself has a relatively low, uniform membrane capacitance. However, the external capacitive load on the proximal and distal portions of the AIS is uneven. On the somatic end, the AIS is connected via axoplasmic resistance to an immense somatodendritic compartment, which diverts a considerable amount of current from the site at which the regenerative depolarization develops by creating a steep, persistent axosomatic voltage gradient during AP initiation. The capacitive load on the distal AIS end, by contrast, is relatively low, as the low-capacitance myelinated segment is expected to depolarize together with the AIS, consuming little current.

Seeking to test the prediction of the model directly, in seven neurons, Na^+ fluxes and spatiotemporal dynamics of AP initiation were measured simultaneously. In these experiments, we opted for paired whole-cell, loose patch recordings as these enable the best amplitude and temporal—and, hence, spatial—resolution for timing of emerging APs (23). Moreover, the loose patch recoding offers an additional advantage in that the recording pipette could be easily moved along the axon, thus allowing AP time detection from multiple sites in sequence. Fig. 2*A* shows averaged Na^+ transients ($n = 25$) and action currents ($n = 50$–200) elicited by single APs in a representative neuron. Action current amplitude was greatest in the proximal AIS, most probably reflecting larger axonal diameter and membrane capacitance. The amplitude of the currents decreased as a function of the distance from the soma; the currents, however, were clearly detectable within the presumed myelinated region (at distances beyond 43 μm in this cell), where no rapidly increasing Na^+ transients were seen in fluorescence recording (14). Measurements of the times of AP onset (Fig. 2*B*) revealed that the APs initiate in the axonal segment significantly less than 10 μm long, located at the distance of 36 to 41 μm from the soma. From this trigger zone, the AP propagates in both directions with apparent conduction velocity of 0.4 m/s, reaching the cell body with a delay of ∼70 μs. Comparison of the AP-elicited ΔF changes within the trigger zone vs. those in more proximal axonal locations (Fig. 2*C*), in an excellent agreement with the model (Fig. 1*C*), indicates that the trigger zone is indeed located within the S_3 subsegment and that the Na^+ flux within the trigger zone boundaries is ∼25% of its maximal value within S_2. Relative mean Na^+ flux in the trigger zone was, on average, $21 \pm 5\%$ ($n = 5$) of the mean S_2 AIS value.

We next sought to understand the role of the position of the depolarizing current source within the AIS on AP initiation by constructing a simplified model with Na^+ channels present in soma, dendrites, and only one of the three AIS subsegments, which were assumed to be of equal length. In the model, increasing Na^+ conductance (gNa) in S_3 was most effective in enhancing the neuronal excitability (Fig. 3*A*) and in shifting AP initiation to the axon (Fig. 3*B*). By contrast, even a threefold S_1:soma gNa ratio was insufficient to create conditions for axonal AP initiation.

It was recently suggested that activity-dependent relocation of the AIS away from the cell body of cultured hippocampal neurons caused a reduction in excitability (24). We tested this idea by varying the S_1 electrotonic parameters in a model in which only S_2 contained Na^+ channels whereas the rest of the membrane remained passive. Contrary to expectations based on passive attenuation of voltage from the soma to the AIS (2), the shorter we made the S_1 segment, the slower the rate of rise of the AP became (Fig. 4*A*) and the more current was required to generate an AP (Fig. 4*B*). This seemingly paradoxical behavior was a result of the decreased isolation of the S_2 segment from the capacitive load

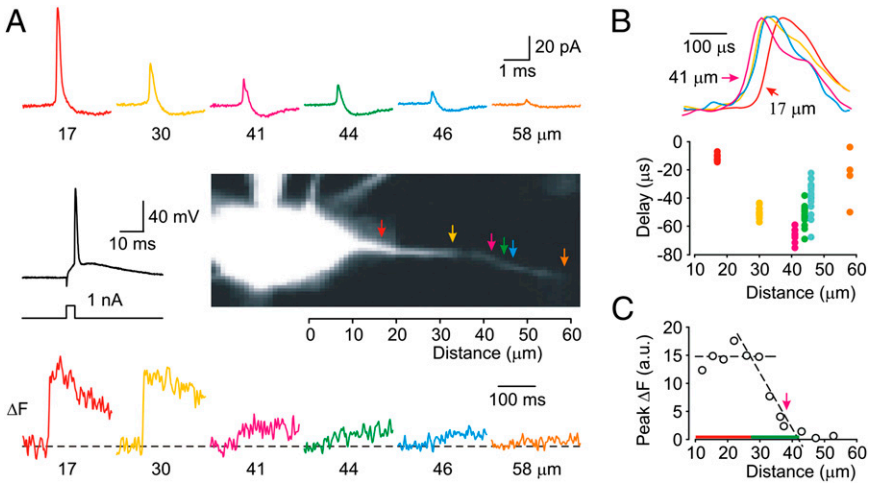

Fig. 2. Spatial mismatch between the Na^+ flux and AP initiation. (*A*) Averaged action currents ($n = 100$–200) and Na^+ transients ($n = 25$) elicited by a single AP at the axonal regions indicated by arrows. The regions are color coded as follows: red, 17 μm from the edge of the soma, as determined from IR differential interference contrast image; yellow, 30 μm; pink, 41 μm; green, 44 μm; blue, 46 μm; and brown, 58 μm. Physiologically, the distal AIS boundary was identified as the location where rapid AP-evoked Na^+ elevation in fluorescence recording became undetectable (43 μm). Note that, at distances beyond this location, in the presumed myelinated region of the axon, Na^+ transient amplitudes were smaller and their peaks were progressively delayed. (*B*) Spatiotemporal pattern of AP initiation. (*Upper*) Normalized action currents recorded from the same locations as in *A* to demonstrate the difference in the delay of their onset. (*Lower*) Delay of AP initiation plotted against distance from the edge of the soma. Each dot corresponds to the mean delay to the onset of the somatic AP ($n =$ 10–40) at a given location, measured at half maximal amplitude. Note that AP initiates in a region located at the distance of 36 to 41 μm from the soma and propagates in both directions with apparent conduction velocity of ∼0.4 m/s. (*C*) Peak fluorescence change: distance plot along the soma–axon axis. Relative S_2 and S_3 position are color-coded as red and green, respectively. Dots are averaged ΔF values from each 5-μm-long segment along the axon during the time interval 2 to 10 ms following the peak of the AP; dashed lines are linear fits to the data. Pink arrow indicates the amplitude of the relative AP-evoked Na^+ flux at the distance of 38 μm from the soma, in the center of the trigger zone, which was ∼25% of the mean S_2 value.

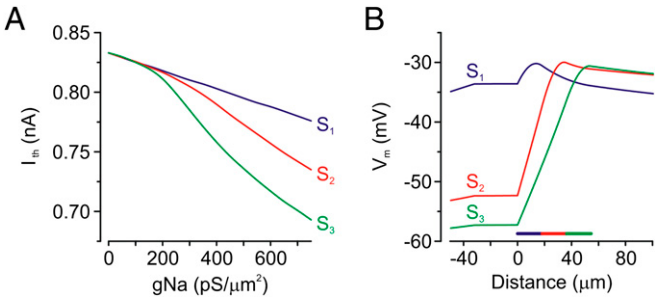

Fig. 3. Implications of depolarizing current source position within the AIS for AP generation. (*A*) Effect of varying Na^+ channel density in the S_1, S_2, and S_3 subsegments on AP current threshold. In a model with Na^+ channels present in only one of the three AIS subsegments, increasing gNa in S_3 is most effective in lowering the amount of current the somatic electrode must deliver to elicit the AP. (*B*) Distal Na^+ channels are most effective in shifting AP initiation to the axon. Voltage-distance plots along the soma–axon axis shown for gNa of 750 pS/μm² in each of the respective subsegments, at a time when the voltage reaches −30 mV. Note that, even with a threefold S_1:soma gNa ratio, the AP initiates simultaneously in the soma and in the axon.

of somatodendritic compartment. Thus, increasing the S_2 isolation by raising axoplasm resistivity in S_1 rescued AP initiation even in the models with the shortest S_1 length. In simulations in which the absolute value of the intracellular resistance of S_1 was held constant, the current threshold increased linearly with S_1 length, in agreement with what is expected from passive soma-to-S_2 attenuation. Our evidence therefore indicates that the most proximal AIS segment serves as a resistive spacer element that ensures proper isolation of the distally located trigger zone from the immense somatodendritic electrical load. At any realistic axoplasm resistivity values [which we assumed to be higher than 80 Ω·cm, the artificial cerebrospinal fluid (ACSF) resistivity (25)], AIS relocation further down the axon would not, by itself, be the reason for a decrease in neuronal excitability (24).

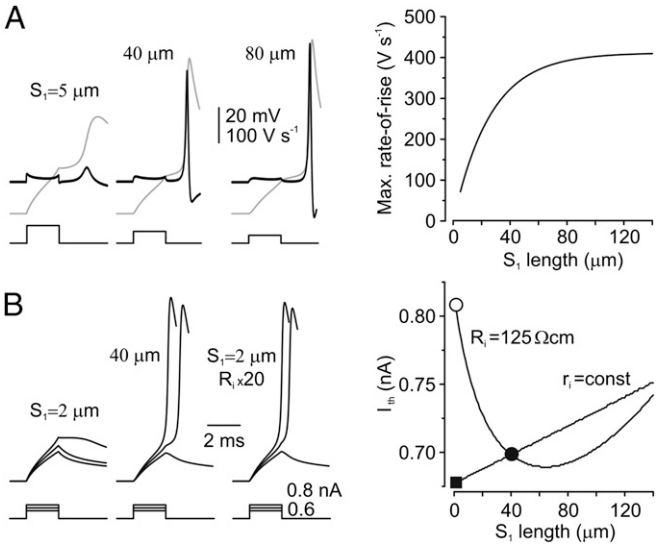

Fig. 4. AP generation critically depends on electrical isolation of the trigger zone from the soma. (*A*) Effect of varying S_1 length on maximal rate of rise of the S_2 AP. In a model in which only S_2 contains Na^+ channels whereas the rest of the neuronal membrane is passive, the amplitude and rate of rise of APs elicited in S_2 by just superthreshold somatic depolarizing current increased with S_1 length. (*Left*) Voltage (gray), dV/dt (black), and current traces for S_1 lengths of 5, 40, and 80 μm. (*Right*) Maximal rate of rise of the S_2 AP increased exponentially as a function of the S_1 length, reflecting a difference in isolation of S_2 from somatodendritic capacitive load. (*B*) Effect of varying S_1 length and resistance on AP initiation. (*Left*) In a model as in *A*, brief current steps in the soma with amplitude of less than 0.8 nA fail to elicit an AP when S_1 is short (2 μm). Current threshold decreases to less than 0.7 nA for S_1 length of 40 μm. A 20-fold increase in axoplasm resistivity in S_1 rescues AP initiation even in the models with the shortest S_1 (2 μm). (*Right*) Varying the S_1 length has a biphasic effect on current threshold. Keeping the S_1 axoplasmic resistance constant by adjusting the axoplasmic resistivity causes the AP current threshold to increase linearly with increase in S_1 length. The circles and the square indicate the S_1 lengths and thresholds for the traces on the left.

Discussion

The spatiotemporal pattern of AP initiation we recorded was qualitatively similar to that reported in earlier studies (1–4). Thus, our electrical data confirm the results obtained by using voltage imaging (1, 4) and whole cell recordings (2, 3) that, in response to orthodromic stimuli, APs in layer 5 pyramidal neurons invariably initiate in the axon, at a distance of 30 to 50 μm from the soma. There exists, however, uncertainty as to where APs initiate relative to the edge of the myelin, which probably reflects the species-, age-, and area-related differences in myelination pattern (1, 3, 26). Comparison of the anatomical and AP latency data for layer 5 pyramidal cells of rat somatosensory cortex yielded a distance of ∼5 μm between the trigger zone and the edge of the myelin (1). We obtained a qualitatively similar result determining the location of the site of the trigger zone and the edge of the myelinated segment in the same neuron. Our assumption that the myelin begins at the site where there is no detectible Na^+ flux seems reasonable, as the consequent length of the initial segment is in close agreement with other reports (1).

We find that Na^+ flux in the trigger zone is approximately four times lower than in the more proximal AIS subsegment, S_2. We suggest this reflects a similar ratio of Na^+ channel densities (i.e., gNa) in the two regions. The precise relationship between the Na^+ flux and gNa is not simple, as it does not seem to have an analytical solution. In an extreme example, the relationship could be quite flat in a spherical compact cell if all the Na^+ conductance is inactivated by the time of the peak of the AP. However, as has been shown experimentally (27, 28), rapidly rising, narrow APs such as those of the AIS have considerable Na^+ conductance during the repolarization phase. In this case, the flux more closely mirrors gNa. Kole et al. (11) studied the Na^+ flux–gNa relationship in models with different AIS-to-proximal basal dendritic Na^+ channel density, and reported that the relationship is nearly linear for a fairly broad range of gNa. They further concluded that relying on the flux data would actually lead to an underestimation of the actual gNa, and hence density differences.

Earlier reports supporting the high current density hypothesis are based mainly on the quantitative evaluation of immunohistochemical data (10–12). Thus, the total Na^+ channel immunofluorescence was found to be maximal (11) or near maximal (10) within the presumed trigger zone in layer 5 pyramidal neurons, although some other studies reported almost constant immunostaining over the AIS length (e.g., ref. 29). Moreover, whereas the density of high-threshold $Na_v1.2$ channels was highest in the proximal AIS, low-threshold $Na_v1.6$ channel staining was most intense within the trigger zone (10). Careful evaluation of $Na_v1.6$ density with EM immunogold staining in CA1 pyramidal neurons revealed that it increases 40 times over the first 10 μm of the AIS length (12). Although the $Na_v1.6$ density within the trigger zone was not estimated, an earlier immunofluorescence study by the same group suggested that it remains constant and high over the entire AIS length (30), including the trigger zone.

These morphological estimates of Na^+ channel density, however, do not always match functional estimates (11, 13, 14), suggesting that many anatomically identifiable Na^+ channels might not be functional. Thus, Na^+ channel currents in excised (13) and attached axonal patches (11), as well as whole-cell currents during local applications of Na^+-rich ACSF to the AIS (11) were less than threefold larger in the trigger zone than in the soma, although

the authors of the latter study (11) presented several arguments why this finding might not be correct. Electrical recordings from blebs that form when cortical axons are cut showed that Na^+ channel density is highest in those blebs that were formed by the presumed trigger zone membrane (10). However, the bleb recordings might differ from the ones in the intact axon, as they could reflect activity of partially proteolyzed channels that have been displaced from the cytoskeleton as a result of axonal injury (31), or their properties could change as result of cytoskeleton disruption (32), and the density estimates could be critically dependent on the accuracy of estimates of the bleb surface area.

In summary, we have directly measured the Na^+ flux within the axonal AP trigger zone of cortical pyramidal neurons. Surprisingly, the flux was significantly lower in the trigger zone than in the middle of the AIS. In the middle region, even though the channel density is higher, the voltage threshold is also higher and APs are generated 20 to 30 μs later than in the trigger zone. Based on these measurements, we propose a model of AP initiation that accounts for measured pattern of Na^+ flux density and for complex electrotonic interactions between the AIS and neighboring compartments. In the model, the electrical load decreases as a function of the distance from the soma, and becomes minimal within the first myelinated internode. Favorable conditions for AP initiation are therefore achieved in the distal AIS portion, close to the edge of myelin, where the ratio of gNa to load is highest. The middle AIS section, where the Na^+ channel density is maximal, might contribute to AP generation by decreasing the capacitive load on the trigger zone. It also plays a critical role in AP backpropagation by providing current, which starts the regenerative depolarization wave in soma and dendrites. Interestingly, our model predicts that relatively small changes in the density of functional Na^+ channels in the distal AIS, or in the electrotonic isolation of the distal AIS by changes in axoplasmic resistivity, would have a strong impact on neuronal excitability.

Methods

Electrophysiology. Experiments were performed on L5 pyramidal neurons in somatosensory neocortical coronal slices prepared from 2- to 8-wk-old CD-1 mice with the use of techniques that are standard in our laboratory (33). Mice were anesthetized with pentobarbital (60 $mg \cdot kg^{-1}$) and decapitated by using procedures approved by the Institutional Animal Care and Use Committee of Ben-Gurion University. Coronal slices (300 μm) from primary somatosensory cortex were cut on a Vibratome (VT1200; Leica) and placed in a holding chamber containing oxygenated ACSF at room temperature; they were transferred to a recording chamber after more than 1 h of incubation. The composition of the ACSF was (in mM): 124 NaCl, 3 KCl, 2 $CaCl_2$, 2 $MgSO_4$, 1.25 NaH_2PO_4, 26 $NaHCO_3$, and 10 glucose; pH 7.4 when bubbled with 95% O_2/CO_2.

The cells were viewed with a 60× water-immersion lens (Olympus) in a BX51WI microscope (Olympus) mounted on an X–Y translation stage (Luigs and Neumann). Somatic whole-cell recordings were made by using patch pipettes pulled from thick-walled borosilicate glass capillaries (1.5 mm outer diameter; Hilgenberg). The pipette solution contained (in mM): 130 K-gluconate, 6 KCl, 2 $MgCl_2$, 4 NaCl, and 10 Hepes, adjusted to pH 7.25 with KOH. Pipettes had resistances of 5 to 7 MΩ when filled with this solution supplemented with 2 mM SBFI (Molecular Probes). Current clamp recordings were made by using an Axoclamp-2A amplifier equipped with an HS-2-x0.01MU headstage (Molecular Devices) in bridge mode; data were low-pass–filtered at 30 kHz (−3 dB, single-pole Bessel filter) and digitized at 100 kHz.

Action currents from visualized axons at distances as far as 100 μm from the soma were obtained simultaneously with whole-cell somatic recordings, in loose patch clamp configuration, by using an Axopatch 200B amplifier (Molecular Devices). Patch pipettes were manufactured from thick-walled borosilicate glass capillaries and had resistances of 10 to 12 MΩ when filled with ACSF. Pipettes were coated to within ~100 μm of the tip with Sylgard (Dow Corning) to minimize the stray capacitance. Currents were low-pass–filtered at 100 kHz (−3 dB, four-pole Bessel filter) and digitized at 200 kHz. Intracellular and extracellular pipette solutions were supplemented with 30 μM Alexa 488 (Molecular Probes) to facilitate axonal patching and to allow superposition of the fluorescence and bright-field images. No sweeps were omitted from the averages, with the exception of rare occurrences when no somatic AP was detected.

All recordings were made at room temperature (21 ± 1 °C). We opted for lower than physiological temperature to slow down AP propagation and to enhance the Na^+ transients (14). Electrophysiological data analysis was accomplished using pCLAMP 7.0 (Axon Instruments), Origin 6.0 (Origin Lab), and Igor Pro 5.05 (Wavemetrics). If not otherwise noted, values are given as mean ± SD. Student *t* test was used for statistical analysis.

Imaging. Imaging experiments were performed as described previously (14) with several technical improvements. SBFI fluorescence was excited by using a high-intensity LED device [385 ± 4 nm; Prizmatix], and the emission was collected by using a modified Olympus U-MNU2 filter set (400-nm dichroic mirror; 420-nm long pass emission filter). Changes in fluorescence were acquired by using a back-illuminated 80 × 80 pixel cooled camera (NeuroCCD-SMQ; RedShirt Imaging) controlled by Neuroplex software. Images were acquired at 500 to 2,000 frames per second. Indicator bleaching was corrected by subtracting an equivalent trace without electrical stimulation.

To improve the signal-to-noise ratio of the traces, 25 to 100 trials were typically averaged. To reduce the photodynamic damage, all positioning and focusing was done by monitoring the fluorescence from the coinjected Alexa 488 by using a high-intensity LED device [480 ± 5 nm; Prizmatix] and modified Olympus U-MNIBA2 filter set or SBFI at lowest LED intensity.

Modeling. Numerical simulations were performed in the NEURON simulation environment (34). Electrophysiological parameters and dynamic $[Na^+]_i$ changes were studied in a simplified compartmental model that encompassed the fundamental morphological and electrical features of layer 5 pyramidal neurons. In the model, the diameter of the proximal AIS section (length, 10 μm) decreased gradually from 3.6 μm in its proximal edge to 1.2 μm in the distal. The rest of the AIS length (48 μm) was of a constant diameter (1.2 μm). The subsequent segment (length, 200 μm; diameter, 1.2 μm) was myelinated. The soma (length, 35 μm; diameter, 23 μm) gave rise to a single apical dendrite (length, 700 μm; diameter, 3.5 μm) and to two basal dendrites (length, 200 μm; diameter, 1.2 μm). For computational precision, all compartments were divided into many segments, with the length of individual segments usually less than 1 μm. Unless otherwise stated, the passive electrical properties R_m, C_m, and R_i were set to 15,000 Ω cm^2, 0.9 μF·cm^{-2}, and 125 Ω·cm, respectively, uniformly throughout all compartments. Myelination was simulated by reducing C_m to 0.02 μF·cm^{-2}. The resting membrane potential at the soma was set to −75 mV. All simulations were run with 5-μs time steps, and the nominal temperature of simulations was 22 °C.

The model incorporated a Hodgkin–Huxley-based Na^+ conductance as previously described (13, 14). The activation time constant was given by $\tau_m = k/[\alpha_m(V_m) + \beta_m(V_m)]$; unless otherwise stated, the scaling factor k was 0.25. Unless otherwise stated, the Na^+ conductance was 250 pS·μm^{-2} in the soma, 200 pS·μm^{-2} in the apical dendrite, and 40 pS·μm^{-2} in the basal dendrites. Myelinated internodes possessed no Na^+ channels. In the model, the steady-state activation and inactivation characteristics of the axonal Na^+ conductance were left-shifted by 6 mV and 3 mV, respectively, compared with the remainder of the neuron. The model included Kv and Kv1-like K^+ channels with kinetics and density as previously described (11). The K^+ equilibrium potential was set to −85 mV. Diffusion of Na^+ was modeled as the exchange of Na^+ ions between adjacent neuronal compartments by using the intrinsic protocols in NEURON assuming a diffusion coefficient of 0.6 μm^2/ms (14). The resting intracellular and the extracellular Na^+ concentrations were set to 4 and 151 mmol/L, respectively.

ACKNOWLEDGMENTS. This research was supported by Israel Science Foundation Grant 1593/10.

1. Palmer LM, Stuart GJ (2006) Site of action potential initiation in layer 5 pyramidal neurons. *J Neurosci* 26(6):1854–1863.
2. Kole MH, Letzkus JJ, Stuart GJ (2007) Axon initial segment Kv1 channels control axonal action potential waveform and synaptic efficacy. *Neuron* 55(4):633–647.
3. Shu Y, Duque A, Yu Y, Haider B, McCormick DA (2007) Properties of action-potential initiation in neocortical pyramidal cells: Evidence from whole cell axon recordings. *J Neurophysiol* 97(1):746–760.
4. Popovic MA, Foust AJ, McCormick DA, Zecevic D (2011) The spatio-temporal characteristics of action potential initiation in layer 5 pyramidal neurons: A voltage imaging study. *J Physiol* 589(Pt 17):4167–4187.
5. Bean BP (2007) The action potential in mammalian central neurons. *Nat Rev Neurosci* 8(6):451–465.
6. Rasband MN (2010) The axon initial segment and the maintenance of neuronal polarity. *Nat Rev Neurosci* 11(8):552–562.

7. Moore JW, Stockbridge N, Westerfield M (1983) On the site of impulse initiation in a neurone. *J Physiol* 336:301–311.
8. Mainen ZF, Joerges J, Huguenard JR, Sejnowski TJ (1995) A model of spike initiation in neocortical pyramidal neurons. *Neuron* 15(6):1427–1439.
9. Yu Y, Shu Y, McCormick DA (2008) Cortical action potential backpropagation explains spike threshold variability and rapid-onset kinetics. *J Neurosci* 28(29):7260–7272.
10. Hu W, et al. (2009) Distinct contributions of Na(v)1.6 and Na(v)1.2 in action potential initiation and backpropagation. *Nat Neurosci* 12(8):996–1002.
11. Kole MH, et al. (2008) Action potential generation requires a high sodium channel density in the axon initial segment. *Nat Neurosci* 11(2):178–186.
12. Lorincz A, Nusser Z (2010) Molecular identity of dendritic voltage-gated sodium channels. *Science* 328(5980):906–909.
13. Colbert CM, Pan E (2002) Ion channel properties underlying axonal action potential initiation in pyramidal neurons. *Nat Neurosci* 5(6):533–538.
14. Fleidervish IA, Lasser-Ross N, Gutnick MJ, Ross WN (2010) Na+ imaging reveals little difference in action potential-evoked Na^+ influx between axon and soma. *Nat Neurosci* 13(7):852–860.
15. Kole MH, Stuart GJ (2012) Signal processing in the axon initial segment. *Neuron* 73(2): 235–247.
16. Colbert CM, Johnston D (1996) Axonal action-potential initiation and Na+ channel densities in the soma and axon initial segment of subicular pyramidal neurons. *J Neurosci* 16(21):6676–6686.
17. Schmidt-Hieber C, Bischofberger J (2010) Fast sodium channel gating supports localized and efficient axonal action potential initiation. *J Neurosci* 30(30):10233–10242.
18. Stuart G, Sakmann B (1995) Amplification of EPSPs by axosomatic sodium channels in neocortical pyramidal neurons. *Neuron* 15(5):1065–1076.
19. Astman N, Gutnick MJ, Fleidervish IA (2006) Persistent sodium current in layer 5 neocortical neurons is primarily generated in the proximal axon. *J Neurosci* 26(13): 3465–3473.
20. Minta A, Tsien RY (1989) Fluorescent indicators for cytosolic sodium. *J Biol Chem* 264(32):19449–19457.
21. Palay SL, Sotelo C, Peters A, Orkand PM (1968) The axon hillock and the initial segment. *J Cell Biol* 38(1):193–201.
22. Naundorf B, Wolf F, Volgushev M (2006) Unique features of action potential initiation in cortical neurons. *Nature* 440(7087):1060–1063.
23. Palmer LM, et al. (2010) Initiation of simple and complex spikes in cerebellar Purkinje cells. *J Physiol* 588(pt 10):1709–1717.
24. Grubb MS, Burrone J (2010) Activity-dependent relocation of the axon initial segment fine-tunes neuronal excitability. *Nature* 465(7301):1070–1074.
25. Savtchenko LP, Rusakov DA (2007) The optimal height of the synaptic cleft. *Proc Natl Acad Sci USA* 104(6):1823–1828.
26. Fariñas I, DeFelipe J (1991) Patterns of synaptic input on corticocortical and corticothalamic cells in the cat visual cortex. II. The axon initial segment. *J Comp Neurol* 304(1):70–77.
27. Carter BC, Bean BP (2009) Sodium entry during action potentials of mammalian neurons: Incomplete inactivation and reduced metabolic efficiency in fast-spiking neurons. *Neuron* 64(6):898–909.
28. Carter BC, Bean BP (2011) Incomplete inactivation and rapid recovery of voltage-dependent sodium channels during high-frequency firing in cerebellar Purkinje neurons. *J Neurophysiol* 105(2):860–871.
29. Inda MC, DeFelipe J, Muñoz A (2006) Voltage-gated ion channels in the axon initial segment of human cortical pyramidal cells and their relationship with chandelier cells. *Proc Natl Acad Sci USA* 103(8):2920–2925.
30. Lorincz A, Nusser Z (2008) Cell-type-dependent molecular composition of the axon initial segment. *J Neurosci* 28(53):14329–14340.
31. Bradke F, Fawcett JW, Spira ME (2012) Assembly of a new growth cone after axotomy: The precursor to axon regeneration. *Nat Rev Neurosci* 13(3):183–193.
32. Aldrich RW, Stevens CF (1987) Voltage-dependent gating of single sodium channels from mammalian neuroblastoma cells. *J Neurosci* 7(2):418–431.
33. Fleidervish IA, Libman L, Katz E, Gutnick MJ (2008) Endogenous polyamines regulate cortical neuronal excitability by blocking voltage-gated Na+ channels. *Proc Natl Acad Sci USA* 105(48):18994–18999.
34. Hines ML, Carnevale NT (1997) The NEURON simulation environment. *Neural Comput* 9(6):1179–1209.